Supplementary Information

Vitamin C modified cathode interlayer for efficient opaque and semitransparent organic photovoltaics

Hailin Yu,[a] Jiayu Wang,*[a] Yingyue Hu,[a] Cenqi Yan,[a] Qichao Ran,[a] and Pei Cheng*[a]

[a] College of Polymer Science and Engineering, National Key Laboratory of Advanced Polymer Materials, Sichuan University, Chengdu 610065, China.

*E-mail: wangjiayu@scu.edu.cn, chengpei@scu.edu.cn

Experimental Section

Materials

PEDOT:PSS (Al4083) was purchased from Heraeus Clevis. PM6, BTP-eC9, L8-BO, PDINN and 2PACz were purchased from HYPER (Zhejiang) Inc. and were used without any further purification. Silver was purchased from ZhongNuo Advanced Material (Beijing) Technology Co., Ltd. Ascorbic acid and other chemicals were purchased from Sigma-Aldrich, Inc.

Molecular modelling

Density functional theory (DFT) calculations were performed with the ORCA 5.0.4 [S1, S2] program using the B3LYP functional [S3, S4] and visualized by VMD.[S5] All-electron split valence basis set with polarization functions def2-SVP was used for all atoms.[S6] The molecules were neutral species with charges set as zero and spin multiplicity set as singlet. Geometry optimizations were performed with full relaxation of all atoms in gas phase without solvent effects. The vibrational frequency calculations were performed to check that the stable structures had no imaginary frequency.

All atomistic MD simulations were performed using the Gromacs–2025.0 software package.[S7] AmberTools–23.6 [S8] was used to generated atom types and the intra- and intermolecular interaction parameters using the general AMBER force field (GAFF2).[S9] The atomic partial charges were obtained by DFT calculations at the B3LYP/def2-SVP level and fitted with the restrained electrostatic potential method.[S10] Missing torsion potentials were reparametrized according to DFT calculations. The simulations were carried out with three-dimensional periodic boundary conditions. The leap-frog integrator with a time step of 2 fs was selected. A spherical cut-off of 1.2 nm for the summation of van der Waals interactions and short-range

Coulomb interactions and the particle-mesh Ewald method for solving long-range Coulomb interactions were used. For PDINN film, the initial geometry was generated by randomly placing 131 PDINN molecules into a box ($8 \times 8 \times 8$ nm^3); for PDINN:VC film, 131 PDINN molecules and 50 VC molecules, corresponding to a 10 wt% content, were randomly placed into the box ($8 \times 8 \times 8$ nm^3) to generate the initial geometry. Energy minimization was then conducted. The films were simulated using the following procedure: (1) 5 ns of simulation at 600 K and 100 bar to quickly bring molecules close together; (2) 10 ns of simulation at 600 K and 1 bar, then cooling to 300 K in 3 ns; (3) 50 ns of equilibration at 300 K and 1 bar. Stochastic cell rescaling barostat [S11] under the NPT ensemble was used to control the pressure for all simulation processes. Velocity rescaling thermostat [S12] was used to control the temperature first, while Nosé–Hoover thermostat [S13, S14] was used for the final 10 ns of equilibration to obtain better equilibrium conformations.

Device fabrication

Opaque devices with structures of ITO/PEDOT:PSS/PM6:BTP-eC9 (10:12 w/w)/PDINN or PDINN:VC/Ag were prepared as following: indium tin oxide (ITO)-coated glasses were cleaned by ultrasonic treatment in detergent, deionized water, acetone and isopropanol for 15 min each, successively. The cleaned ITO substrates were then treated with ultraviolet-ozone for 20 min before used. PEDOT:PSS was spin-coated on the ITO substrates at 3500 rpm followed by annealed at 150 °C for 20 min in air. Then the samples were transferred into a nitrogen-filled glovebox. PM6:BTP-eC9 (10:12 mg mL^{-1} with 0.6 vol% 1, 8-diiodooctane additive and chlorobenzene solvent) was spin-coated on PEDOT:PSS layer, and annealed at 100 °C for 5 min. Then PDINN solutions (1 mg mL^{-1} in methanol) containing different concentrations of

VC were spin-coated at 3000 rpm for 60 s. Finally, 150 nm Ag were thermal evaporated on the PDINN with a thermal evaporation rate of 3 Å s^{-1}. Opaque devices with structures of ITO/2PACz/active layer/PDINN or PDINN:VC/Ag are prepared as following: 2PACz solutions (0.5 mg mL^{-1} ethanol) were spin-coated on the ITO substrates at 3000 rpm for 60 s. Then D18:L8-BO (4.5:4.5 mg mL^{-1} in chloroform) or PM6:L8-BO (7:8.4 mg mL^{-1} in chloroform) were spin-coated at 1500 rpm or 2500 rpm on 2PACz and annealed at 100 °C for 2 min. Subsequently, PDINN solutions (1 mg mL^{-1} in methanol) containing 0.1 mg mL^{-1} of VC were spin-coated at 3000 rpm for 60 s. Finally, 150 nm Ag were thermal evaporated on the PDINN with a thermal evaporation rate of 3 Å s^{-1}. The semi-transparent devices with structures of ITO/PEDOT:PSS/PM6:BTP-eC9/PDINN:VC/Ag were prepared as follows: the ratios of PM6:BTP-eC9 were 10:12 mg mL^{-1}, 8:12 mg mL^{-1}, 6:12 mg mL^{-1} and 4:12 mg mL^{-1} and the Ag electrode thicknesses were 30 nm, 25 nm, 20 nm, 15 nm, 10 nm and 8 nm, respectively. Other preparation procedures were consistent with that of the opaque devices. Finally, 35 nm MoO_3 was thermal evaporated at a rate of 0.1 Å s^{-1} as the optical structure. The effective area of all devices is 3.90 mm^2.

Characterization

The morphology was analysed using field emission scanning electron microscope (FESEM, Apreo S HiVoc). X-ray photoelectron spectroscopy (XPS) was conducted on a Kratos AXIS Supra photoelectron spectrometer. Transmittance spectra were measured on a Shimadzu UV-2600i spectrophotometer. *J–V* characteristics were measured by using a computer-controlled Keysight B2901A Source Meter under the illumination of an Enlitech solar simulator (SS-X50, AAA grade) coupled with AM 1.5G solar spectrum filters. The EQE spectra were measured

using a Solar Cell Spectral Response Measurement System QE-R (Enlitech Co., Ltd.). The light stability test was conducted on optimized unencapsulated devices in a glove box filled with nitrogen under continuous light illumination and maximum power point tracking. A white LED sunlight simulator was used as the light source (spectral region: 420-940 nm, Shenzhen Lancheng Technology Co., Ltd., LED-80) with an intensity equivalent to 1 sun. The electrochemical testing was performed by electrochemical workstation (Gamry reference 620 Potentiostat). The contact angles of water (H_2O) and diiodomethane (DIM) on PDINN and PDINN:VC films were measured by a video optical contact angle meter (DSA-100 (KRUSS Germany)) and the surface free energies of the films were calculated using the Owens-Wendt-Rabel-Kaelble (OWRK) method. The OWRK calculation formula is given below:

$$\gamma_L (1 + \cos\theta) = 2\sqrt{\gamma_s^d \times \gamma_L^d} + 2\sqrt{\gamma_s^p \times \gamma_L^p}$$

$$\gamma_L = \gamma_L^d + \gamma_L^p$$

$$\gamma_s = \gamma_s^d + \gamma_s^p$$

where θ is the contact angle, γ_s is the surface energy of the solid, γ_L is the surface energy of the liquid, and γ_d and γ_p are the dispersive and polar surface energies, respectively.

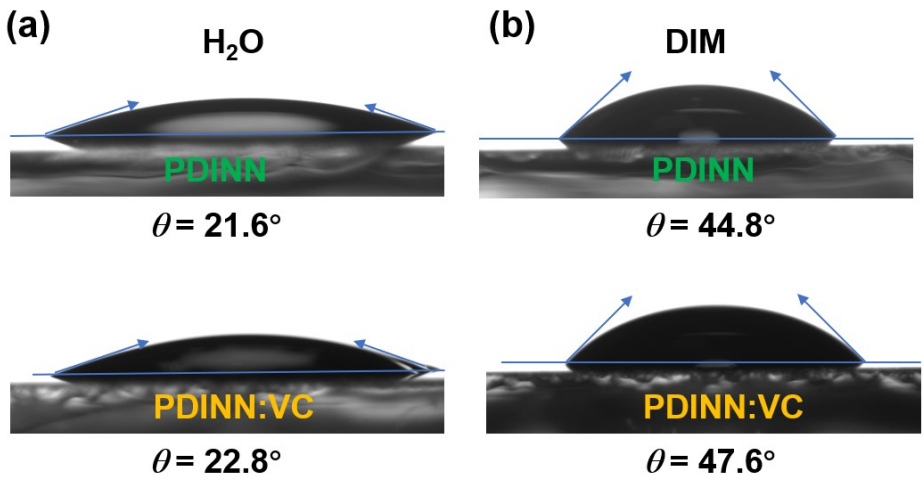

Fig. S1 Contact angles of (a) H_2O and (b) DIM droplets on PDINN and PDINN:VC films.

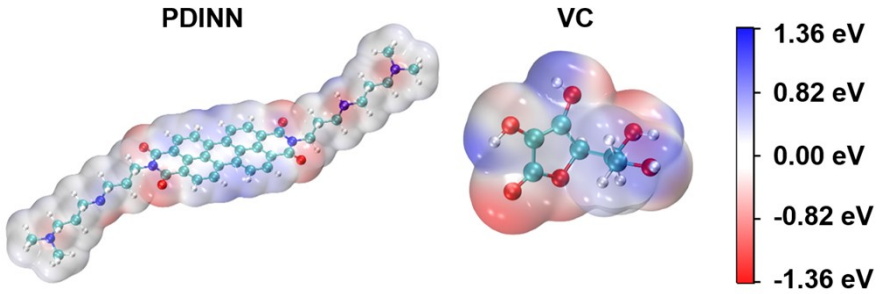

Fig. S2 Electrostatic potential maps of PDINN and VC.

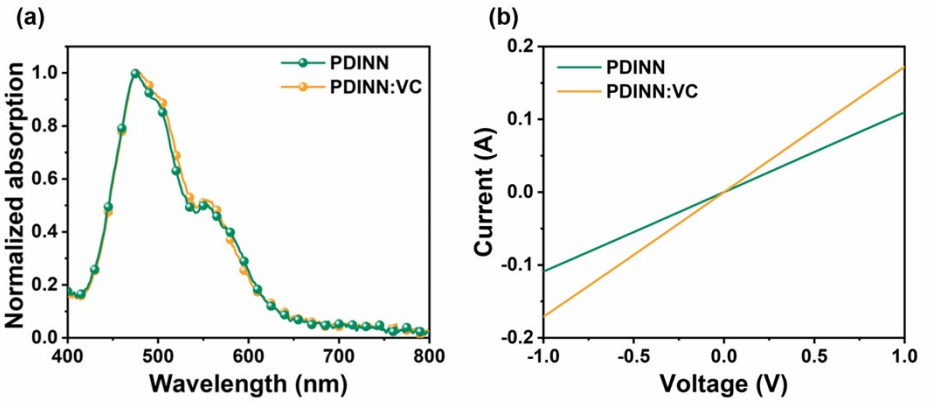

Fig. S3 (a) Absorption spectra of PDINN and PDINN:VC films. (d) The *I-V* curves of ITO/PDINN or PDINN:VC/Ag.

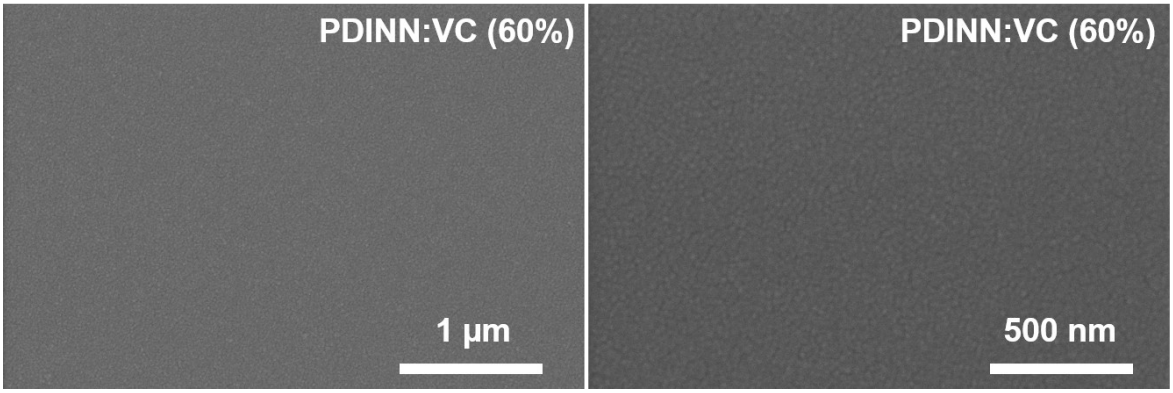

Fig. S4 SEM morphology of PDINN:VC (60%) films.

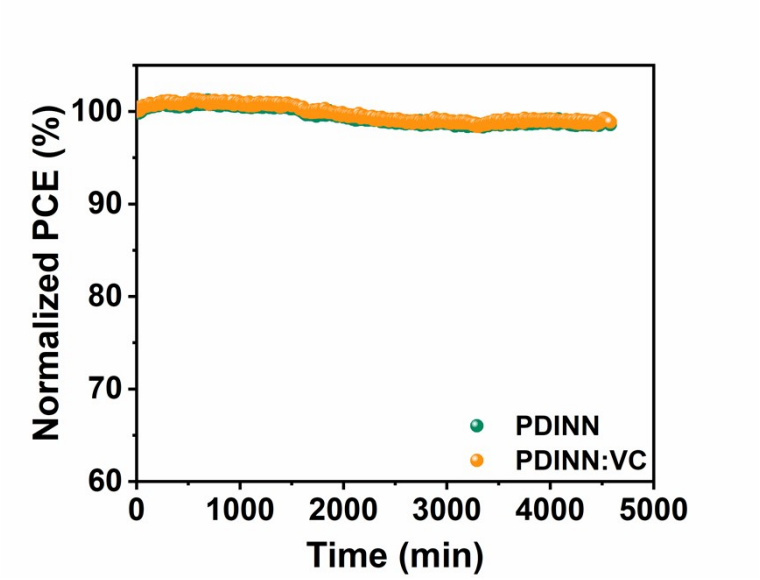

Fig. S5 PCE changes of PDINN and PDINN:VC based devices over time under MPP testing.

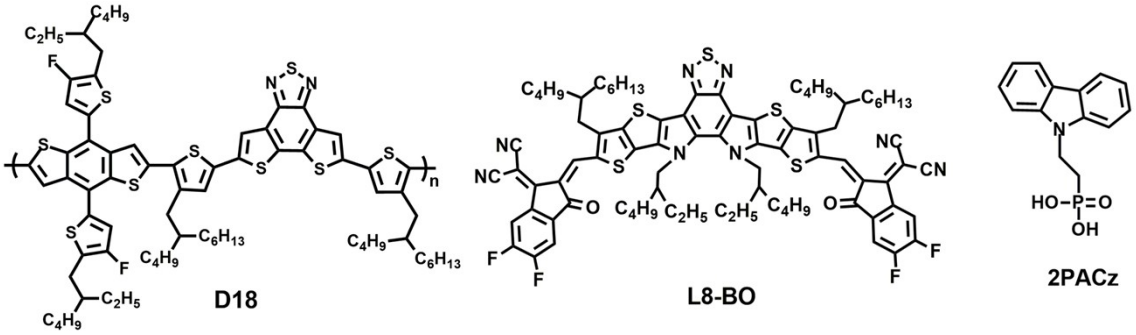

Fig. S6 The chemical structures of D18, L8-BO and 2PACz.

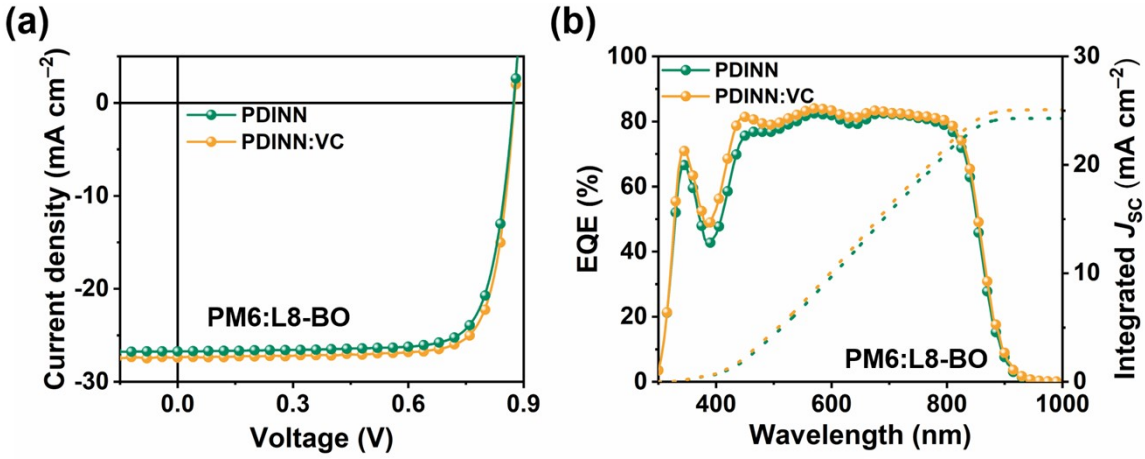

Fig. S7 *J-V* curves and EQE spectra of the optimal devices based on PM6:L8-BO.

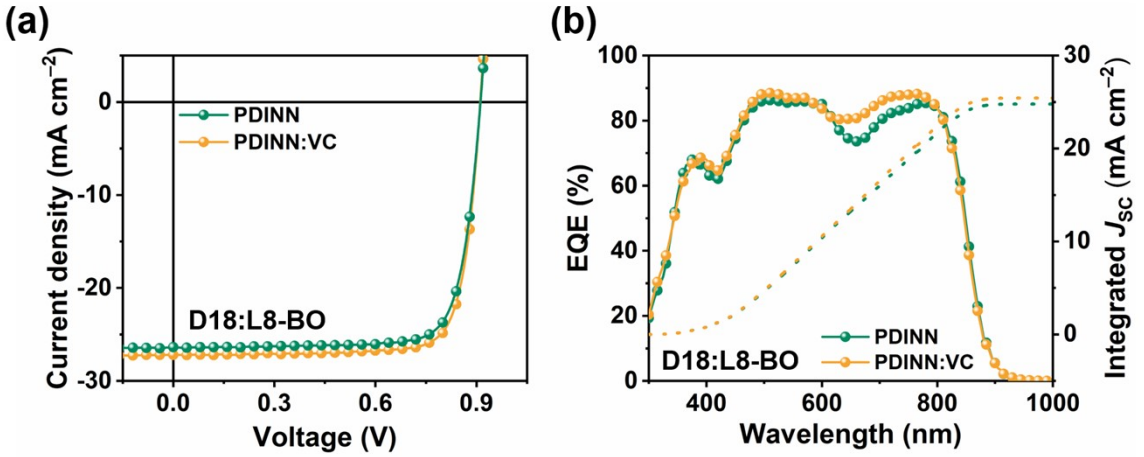

Fig. S8 *J-V* curves and EQE spectra of the optimal devices based on D18:L8-BO.

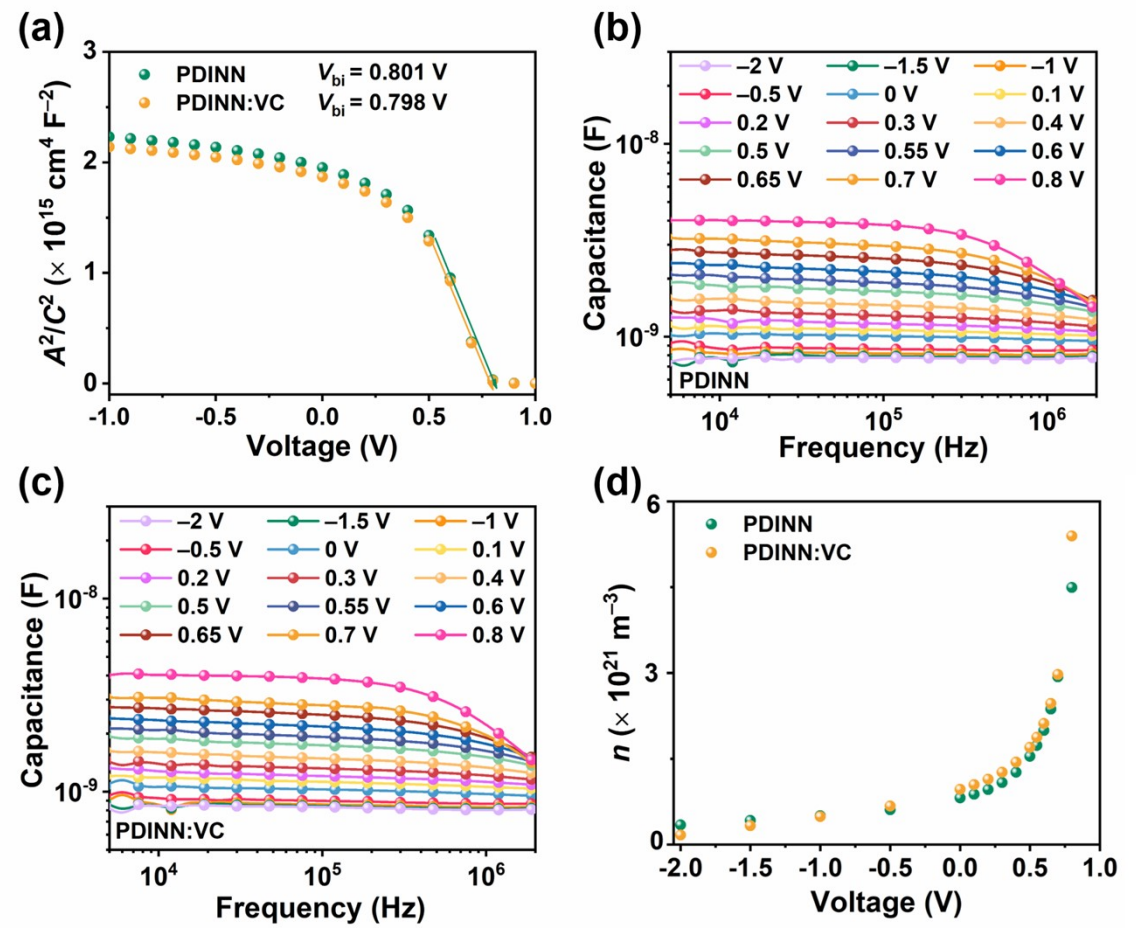

Fig. S9 (a) Mott-Schottky curves of the devices. Capacitance-frequency plots of (b) PDINN-based device and (c) PDINN:VC-based device at different bias voltages under AM 1.5G (100 mW cm^{-2}) illumination. (d) Carrier density of the devices at different bias voltages.

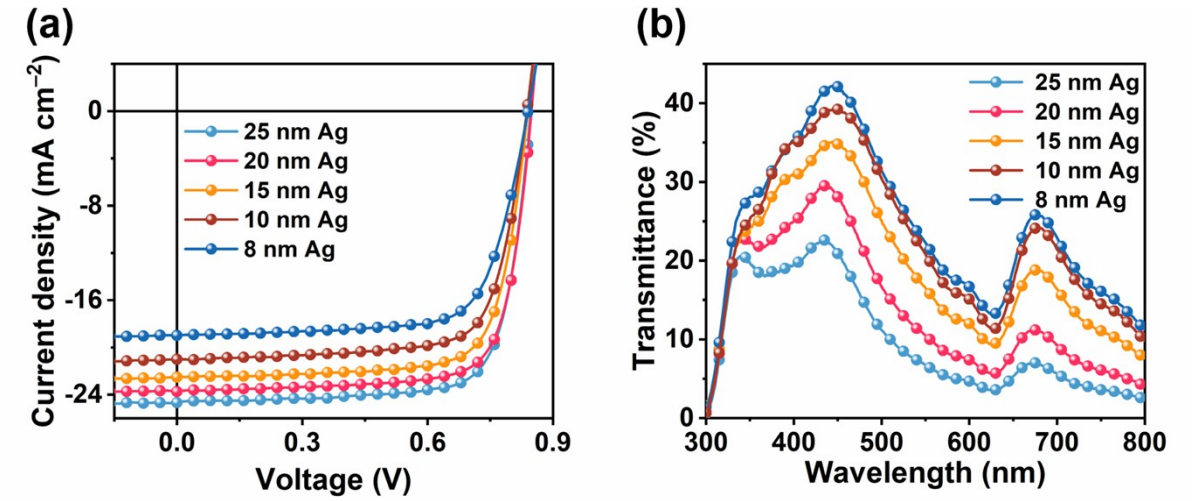

Fig. S10 (a) *J-V* curves and (b) transmittance spectra of STOPVs based on different Ag electrode thicknesses.

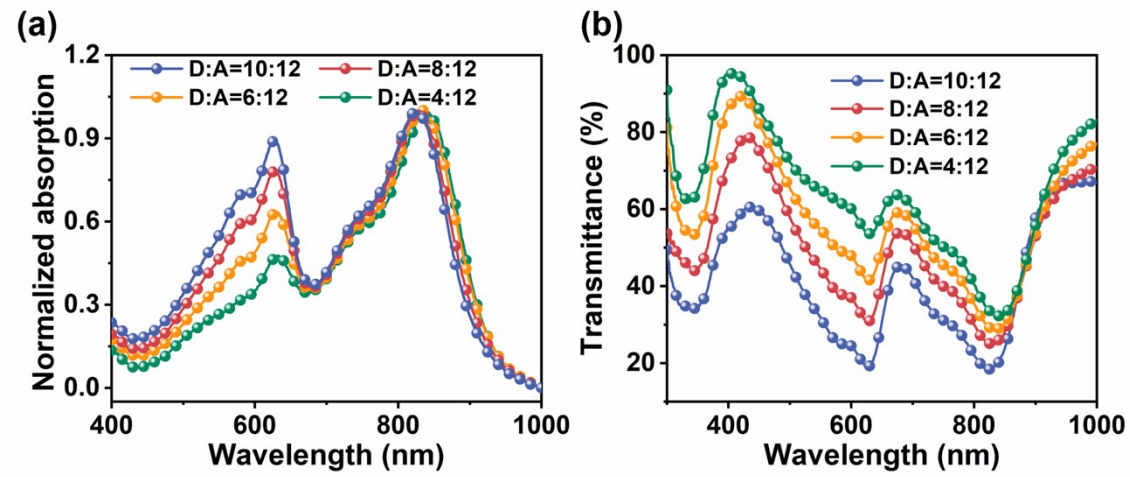

Fig. S11 (a) Normalized absorption spectra and (b) transmittance spectra of PM6:BTP-eC9 films at different D:A ratio.

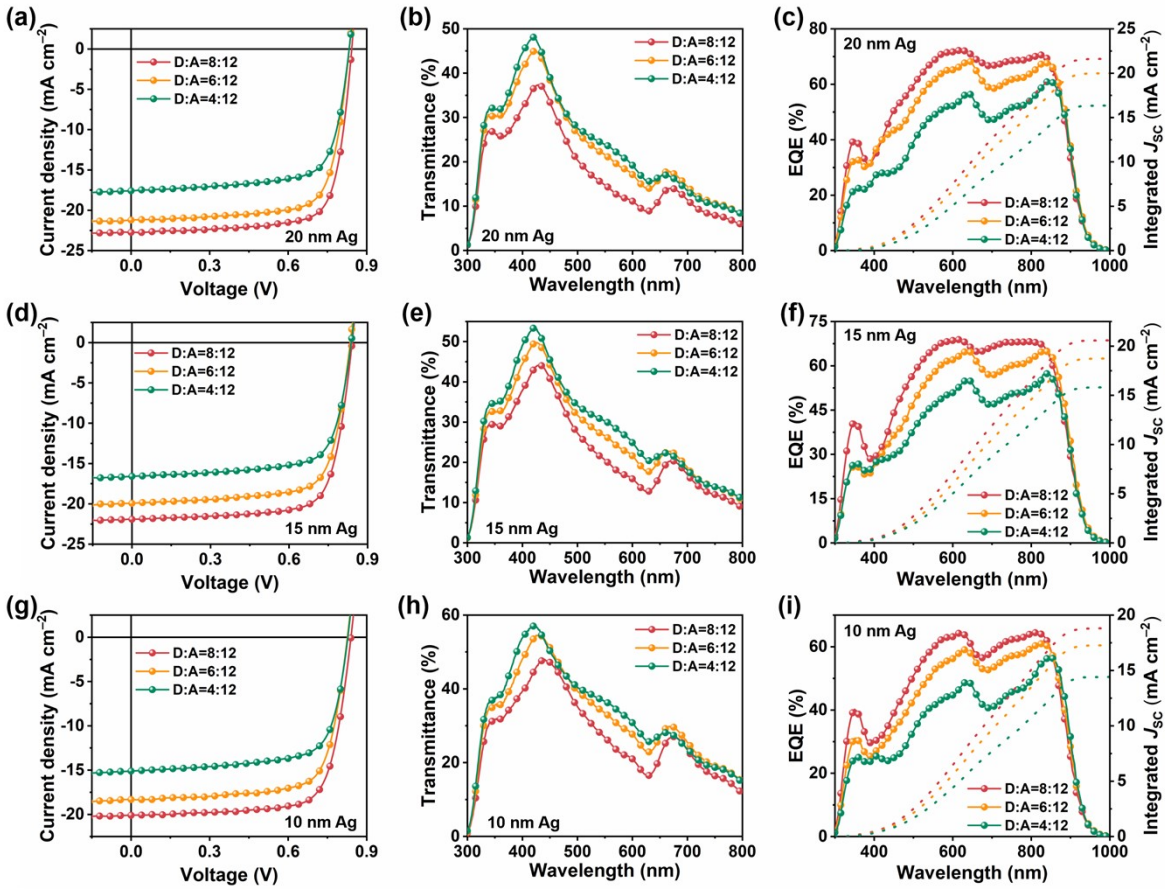

Fig. S12 (a) *J-V* curves, (b) transmittance spectra and (c) EQE spectra of STOPVs based on 20 nm Ag electrode at different D:A ratio. (d) *J-V* curves, (e) transmittance spectra and (f) EQE spectra of STOPVs based on 15 nm Ag electrode at different D:A ratio. (g) *J-V* curves, (h) transmittance spectra and (i) EQE spectra of STOPVs based on 10 nm Ag electrode at different D:A ratio.

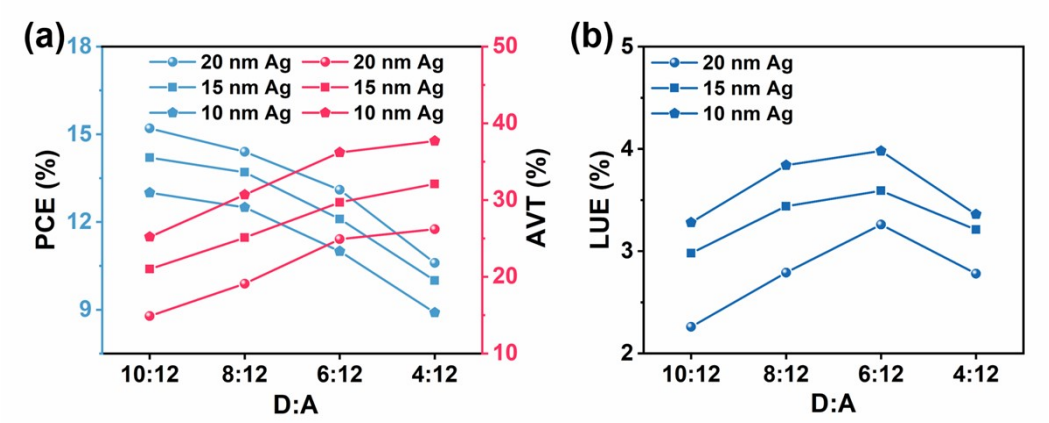

Fig. S13 (a) Variation curves of PCE and AVT with D:A ratio. (b) Variation curves of LUE with D:A ratio.

Table S1 Contact angles of H_2O and DIM on PDINN and PDINN:VC films and the calculated surface energy of the corresponding films.

CIL	H_2O Contact Angle* (°)	DIM Contact Angle* (°)	Surface Energy (mN/m)
PDINN	21.6	44.8	71.3
PDINN:VC	22.8	47.6	70.0

*DIM: $\gamma_L^P = 0$ mJ/m^2, $\gamma_L^d = 50.8$ mJ/m^2; H_2O: $\gamma_L^P = 51.0$ mJ/m^2, $\gamma_L^d = 21.8$ mJ/m^2.

Table S2 Photovoltaic performance parameters of opaque devices based on PM6:BTP-eC9 at different VC contents.

Content of VC	V_{OC} (V)[a]	J_{SC} (mA cm^{-2})[a]	FF (%)[a]	PCE (%)[a]
0%	0.849 (0.846±0.002)	26.6 (26.7±0.4)	76.3 (75.5±1.1)	17.2 (17.0±0.2)
5%	0.847 (0.846±0.002)	26.8 (26.7±0.3)	76.6 (75.9±1.0)	17.4 (17.1±0.2)
10%	0.849 (0.848±0.002)	27.3 (27.1±0.5)	76.7 (76.3±0.9)	17.8 (17.6±0.2)
20%	0.847 (0.848±0.003)	26.8 (26.8±0.2)	77.2 (76.3±0.7)	17.5 (17.3±0.2)
40%	0.850 (0.846±0.004)	26.7 (26.7±0.3)	76.3 (75.7±0.8)	17.3 (17.1±0.2)
60%	0.821 (0.816±0.003)	26.2 (25.9±0.4)	70.2 (68.8±1.3)	15.1 (14.5±0.4)

[a] The values of each parameter in parentheses are the mean and standard deviation calculated from eight devices.

Table S3 Photovoltaic performance parameters of opaque devices based on D18:L8-BO.

CIL	V_{OC} (V)[a]	J_{SC} (mA cm^{-2})[a]	FF (%)[a]	PCE (%)[a]
PDINN	0.910 (0.908±0.003)	26.4 (26.2±0.3)	79.2 (78.9±1.0)	19.0 (18.7±0.2)
PDINN:VC	0.909 (0.912±0.003)	27.2 (26.8±0.3)	80.1 (79.9±0.5)	19.8 (19.5±0.2)

[a] The values of each parameter in parentheses are the mean and standard deviation calculated from eight devices.

Table S4 Photovoltaic performance parameters of STOPVs at different Ag electrode thicknesses.

Electrode thickness	V_{OC}[a] (V)	J_{SC}[a] (mA cm^{-2})	FF[a] (%)	PCE[a] (%)	AVT[b] (%)	LUE (%)
25 nm	0.846 (0.842±0.003)	24.6 (24.5±0.4)	75.8 (75.1±1.0)	15.8 (15.5±0.3)	10.3	1.63
20 nm	0.847 (0.842±0.004)	23.7 (23.9±0.3)	76.1 (74.7±0.9)	15.2 (15.0±0.2)	14.9	2.26
15 nm	0.839 (0.842±0.004)	22.5 (22.4±0.3)	75.1 (74.5±0.8)	14.2 (14.0±0.2)	21.0	2.98
10 nm	0.837 (0.837±0.004)	21.0 (20.6±0.4)	73.8 (74.3±0.6)	13.0 (12.8±0.2)	25.2	3.28
8 nm	0.835 (0.830±0.004)	19.1 (19.0±0.2)	71.7 (70.6±1.1)	11.4 (11.1±0.3)	26.8	3.06

[a] The values of each parameter in parentheses are the mean and standard deviation calculated from eight devices.

[b] AVT is obtained by calculating the arithmetic mean of the transmittance between 400~700 nm.

Table S5 Photovoltaic performance parameters of STOPVs at different Ag electrode thicknesses and D:A ratio.

Electrode thickness	D:A ratio	V_{OC}[a] (V)	J_{SC}[a] (mA cm^{-2})	FF[a] (%)	PCE[a] (%)	AVT[b] (%)	LUE (%)
20 nm	8:12	0.842 (0.846±0.003)	22.7 (21.9±0.5)	75.5 (75.2±0.6)	14.4 (14.0±0.3)	19.1	2.79
	6:12	0.832 (0.835±0.004)	21.2 (20.5±0.8)	74.1 (74.3±0.3)	13.1 (12.7±0.4)	24.9	3.26
	4:12	0.832 (0.830±0.003)	17.6 (17.0±0.9)	72.4 (72.0±0.6)	10.6 (10.2±0.4)	26.2	2.78
15 nm	8:12	0.841 (0.839±0.006)	21.9 (21.7±0.5)	74.2 (74.4±0.7)	13.7 (13.4±0.2)	25.1	3.44
	6:12	0.833 (0.833±0.005)	19.9 (19.2±0.6)	73.1 (73.0±0.6)	12.1 (11.7±0.3)	29.7	3.59
	4:12	0.836 (0.831±0.004)	16.6 (16.4±0.5)	72.1 (70.6±1.5)	10.0 (9.6±0.3)	32.1	3.21
10 nm	8:12	0.839 (0.834±0.005)	20.1 (20.2±0.4)	74.0 (73.0±0.7)	12.5 (12.3±0.2)	30.7	3.84
	6:12	0.826 (0.828±0.002)	18.3 (17.7±0.6)	72.9 (72.7±0.1)	11.0 (10.6±0.4)	36.2	3.98
	4:12	0.826 (0.824±0.002)	15.1 (14.8±0.5)	71.1 (71.1±0.1)	8.9 (8.7±0.3)	37.7	3.36

[a] The values of each parameter in parentheses are the mean and standard deviation calculated from eight devices.

[b] AVT is obtained by calculating the arithmetic mean of the transmittance between 400~700 nm.

Table S6 Detailed parameters of STOPVs reported in the literatures.

Reference	Optical structure	PCE (%)	AVT (%)	LUE (%)
This work	w/o	11.0	36.2	3.98
This work	w	12.1	37.4	4.53
S15	w/o	11.53	30.23	3.48
S15	w	10.10	35.82	3.62
S16	w/o	12.42	24.42	3.03
S16	w	12.50	32.05	4.06
S17	w/o	9.81	38.91	3.82
S17	w	9.03	43.15	3.90
S18	w/o	14.66	27.40	4.02
S18	w	16.14	33.02	5.33
S19	w/o	13.50	27.23	3.68
S19	w	15.19	30.57	4.64
S20	w/o	10.39	29.25	3.04
S20	w	9.33	43.08	4.02
S21	w/o	12.78	21.00	2.68
S21	w	11.18	32.07	3.59
S22	w/o	9.20	39.47	3.63
S22	w	9.93	40.36	4.01
S23	w/o	11.47	24.6	2.82
S23	w	13.15	25.9	3.41
S24	w/o	5.9	44	2.6
S24	w	8.3	46	3.8

References

S1. F. Neese, *WIREs Comput. Mol. Sci.*, 2012, **2**, 73-78.

S2. F. Neese, *WIREs Comput. Mol. Sci.*, 2022, **12**, e1606.

S3. C. Lee, W. Yang and R. G. Parr, *Phys. Rev. B*, 1988, **37**, 785-789.

S4. A. D. Becke, *J. Chem. Phys.*, 1993, **98**, 5648-5652.

S5. W. Humphrey, A. Dalke and K. Schulten, *J. Mol. Graph.*, 1996, **14**, 33-38.

S6. F. Weigend and R. Ahlrichs, *Phys. Chem. Chem. Phys.*, 2005, **7**, 3297-3305.

S7. M. J. Abraham, T. Murtola, R. Schulz, S. Páll, J. C. Smith, B. Hess and E. Lindahl, *SoftwareX*, 2015, **1-2**, 19-25.

S8. D. A. Case, H. M. Aktulga, K. Belfon, D. S. Cerutti, G. A. Cisneros, V. W. D. Cruzeiro, N. Forouzesh, T. J. Giese, A. W. Götz, H. Gohlke, S. Izadi, K. Kasavajhala, M. C. Kaymak, E. King, T. Kurtzman, T.-S. Lee, P. Li, J. Liu, T. Luchko, R. Luo, M. Manathunga, M. R. Machado, H. M. Nguyen, K. A. O'Hearn, A. V. Onufriev, F. Pan, S. Pantano, R. Qi, A. Rahnamoun, A. Risheh, S. Schott-Verdugo, A. Shajan, J. Swails, J. Wang, H. Wei, X. Wu, Y. Wu, S. Zhang, S. Zhao, Q. Zhu, T. E. Cheatham III, D. R. Roe, A. Roitberg, C. Simmerling, D. M. York, M. C. Nagan and K. M. Merz Jr. AmberTools. *J. Chem. Inf. Model.*, 2023, **63**, 6183-6191.

S9. J. Wang, R. M. Wolf, J. W. Caldwell, P. A. Kollman and D. A. Case, *J. Comput. Chem.*, 2004, **25**, 1157-1174.

S10. C. I. Bayly, P. Cieplak, W. Cornell and P. A. Kollman, *J. Phys. Chem.*, 1993, **97**, 10269-10280.

S11. M. Bernetti and G. Bussi, *J. Chem. Phys.*, 2020, **153**, 114107.

S12. G. Bussi, D. Donadio and M. Parrinello, *J. Chem. Phys.*, 2007, **126**, 014101.

S13. S. Nosé, *J. Chem. Phys.*, 1984, **81**, 511-519.

S14. W. G. Hoover, *Phys. Rev. A*, 1985, **31**, 1695-1697.

S15. S. Li, L. Xiao, H. Zhang, Y. Zhang, W. Zhang, H. Zhou and Y. Zhang, *Nano Lett.*, 2025, **25**, 5316-5324.

S16. N. Zhang, Z. Zhou, Y. An, F. Qi, R. Xia, G. Du, T. Xia, L. Ke, N. Li, F. R. Lin, A. K.

Jen and H.-L. Yip, *Adv. Energy Mater.*, 2025, **15**, 2404129.

S17. J. Yu, X. Liu, J. Zhou and G. Li, *Adv. Funct. Mater.*, 2024, **34**, 2406070.

S18. T. Xu, B. Deng, K. Zheng, H. Li, Z. Wang, Y. Zhong, C. Zhang, G. Lévêque, B. Grandidier, R. Bachelot, M. Treguer-Delapierre, Y. Qi and S. Wang, *Adv. Mater.*, 2024, **36**, 2311305.

S19. B. Deng, K. Zheng, Z. Wang, L. Yin, H. Dong, C. Zhang, M. Treguer-Delapierre, K. N'konou, B. Grandidier, S. Wang, J. Zhang and T. Xu, *ACS Energy Lett.*, 2024, **9**, 976-984.

S20. X. Xu, Q. Wei, Z. Zhou, H. He, J. Tian, H.-L. Yip, Y. Fu, X. Lu, Y. Zhou, Y. Li and Y. Zou, *Adv. Funct. Mater.*, 2023, **34**, 2305017.

S21. D. Wang, Y. Li, G. Zhou, E. Gu, R. Xia, B. Yan, J. Yao, H. Zhu, X. Lu, H.-L. Yip, H. Chen and C.-Z. Li, *Energy Environ. Sci.*, 2022, **15**, 2629-2637.

S22. X. Wu, S. Liu, H. Li, X. Meng, X. Hu, R. Guo and Y. Chen, *Adv. Opt. Mater.*, 2022, **10**, 2201803.

S23. T. Xu, Y. Luo, S. Wu, B. Deng, S. Chen, Y. Zhong, S. Wang, G. Leveque, R. Bachelot and F. Zhu, *Adv. Sci.*, 2022, **9**, 2202150.

S24. H. K. M. Sheriff, Y. Li, B. Qu and S. R. Forrest, *Appl. Phys. Lett.*, 2021, **118**, 033302.